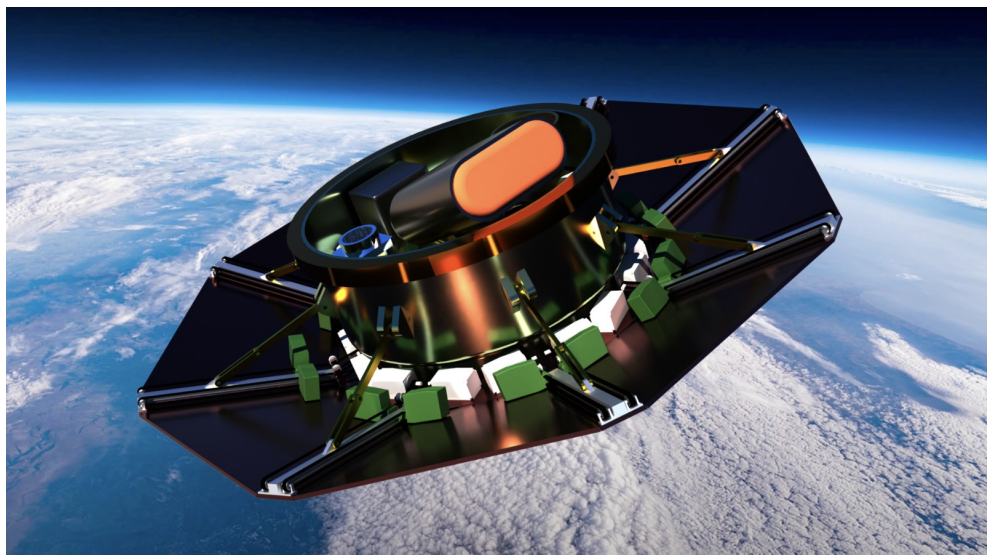




FOLDABLE AEROSHELL DEMONSTRATOR

Space HAVEN: Design of Command & Data Handling and Telemetry Subsystems

FAD06 - Demonstrator Subsystem Design



Student: Chris Ziyi Yao

CID: 01908293

Date: 19/06/23

Academic Responsible: Dr Paul Bruce
Supervisor: Dr Paul Bruce

Department: Department of Aeronautics
Course: MEng Aeronautical Engineering
Module: AERO60004 - Group Design Project
Academic Year: 2022/2023

Department of Aeronautics
South Kensington Campus
Imperial College London
London. SW7 2AZ.
U.K.

Abstract

This report presents a comprehensive design of the Command and Data Handling (C&DH) and Telemetry Tracking and Command (TT&C) subsystems. The C&DH subsystem design was based on a rigorous data budget analysis, incorporating all components, including sensors and actuator control commands. The SpaceWire bus was selected for its flexible, high-data-rate, and low-power-consumption attributes. Accompanying the bus were the Real-time Operating System (RTOS) RTEMS and the LEON processor series. The report includes a detailed schematic illustrating communication paths and task distributions among processors, mass memory modules, and instruments. Leveraging Commercial off-the-shelf (COTS) components, the C&DH subsystem achieved a Technology Readiness Level (TRL) of 7.

For the TT&C subsystem aiming at TRL of 5, communication downlink losses and shifts were quantitatively analysed in line with the demonstrator mission profile. The Gaussian Minimum Shift Keying (GMSK) and Pseudo Noise (PN) Ranging modulation method was applied. The report further features a practical design of the ground station receiver, modelled in Simulink, incorporating a Proportional-Integral (PI) controller to correct for Doppler shifts. The collective design choices and analyses result in a robust system architecture with high performance, ensuring successful testing of the mission.

FAD22: Space HAVEN

Sub-Group	Name	CID
FAD01 - Project Co-ordination	Amy-Beth Curtis	01859027
	Eunice Lam	01861076
	Shapol M	01865267
FAD02 - Mission Design & Analysis	Joshua Goldspink	01870028
	Gul Kaur	01905296
	William Taylor	01771592
	Usmaan Yaqoob	01847219
FAD03 - Launcher Structural Design	Myka Abaquin	01857878
	Kunpeng Li	01909532
	Julian Ting	01843067
	Yichen You	01863827
FAD04 - Launcher Subsystem Design	Nicolas Bayle	01943039
	Lara Couceiro Alves	01877828
	Pablo Duhamel	01915106
	Artem Sheykin	01913084
FAD05 - Demonstrator Structural Design	Harry Allcock	01854056
	Imsara Samarasinghe	01949330
	Timur Uyumaz	01906145
	Raine Wong	01876352
FAD06 - Demonstrator Subsystem Design	Paula Gutierrez	01949543
	Cristian Vegas Medina	01874108
	Sevan Vlieghe	01926818
	Chris Ziyi Yao	01908293
FAD07 - Launcher & Demonstrator Aerodynamic Analysis	Yuzhe Dun	01849823
	Nathanael Jenkins	01843784
	Mohammad Kapadia	01862576
	Joel Tomas Pimentel	01881299

Contents

List of Figures	iv
List of Tables	v
List of Symbols	vi
List of Abbreviations	vi
1 Introduction	1
2 Command & Data Handling (C&DH) Subsystem	1
2.1 Design Objectives and Requirements	1
2.2 Data Budget Estimations	1
2.3 Bus, Operating System (OS), and Processors	3
2.4 System Integrations	3
3 Telemetry Tracking & Command (TT&C) Subsystem	5
3.1 Design Objectives and Requirements	5
3.2 Reentry Environment and Atmospheric Conditions	6
3.3 System Architecture	7
3.4 Communication Channel	7
3.5 Data Modulation Method: GMSK	8
3.6 Ground Receiver Design	9
4 Discussions and Future Works	11
4.1 C&DH Subsystem	11
4.2 TT&C Subsystem	12
5 Conclusion	12
References	13
Appendix	16

List of Figures

1	Demonstrator Mission Profile	1
2	SpaceWire Data Packet Format	3
3	SpaceWire's Point-to-point Link	4
4	Purely Point-to-Point Link Connections Between Nodes	4
5	SpaceWire's Router-Based Architecture	4
6	C&DH Subsystem Architecture	5
7	Required carrier frequency to penetrate the plasma sheath at a given Electron density	6
8	Radiowave Attenuation vs Electron Density	6
9	High-level TT&C System Architecture	7
10	Free space loss vs Mission time	8
11	Doppler Shift vs Mission Time	8
12	Atmospheric Attenuation vs Mission Time	8
13	GMSK Data Modulation Method	9
14	Encoded data signal transmitted and encoded signal data received at ground station with a delay	9
15	Power Spectral Density (dBm) Snippets of Before (yellow) and After the Downlink Process (blue)	10
16	Definition of Noise Temperature [1]	10
17	Ground Station Design in Simulink	11
18	Power Spectral Density (dBm) after Doppler Corrections	11
19	Attenuation due to Plasma Penetration vs Altitude for NASA's RAM mission	17
20	Specific Attenuation vs Carrier Frequency	17
21	Demonstrator Reentry Trajectory from Mission Analysis Team	18

List of Tables

1	List of data considered in data budget estimations	2
2	Data rate and total data size estimations	3
3	Comparison of Different Bus Systems	16

List of Symbols

ω_p	Plasma frequency (rad/s)
n_e	Electron number density (cm^{-3})
e	Elementary charge (C)
m_e	Electron mass (kg)
ϵ_0	Electric constant in free space (F/m)
α	Plasma attenuation (dB/m)
k_0	Free space wave number
ν	Plasma collision frequency (rad/s)
T_p	Plasma temperature (K)
f_o	Observer (ground station) frequency (Hz)
f_s	Source (carrier) frequency (Hz)
f_c	Carrier frequency (Hz)
v_o	Observer (ground station) speed (m/s)
v_s	Source (carrier) speed (m/s)
c	Speed of light (m/s)
L_s	Free space loss (dB)
r	Distance between demonstrator and ground station (m)
N''_{oxygen}	Imaginary parts of the complex refractivities of oxygen
$N''_{\text{water vapor}}$	Imaginary parts of the complex refractivities of water vapor
N''_D	Imaginary parts of the complex refractivities of pressure-induced nitrogen
S_i	Strength of i_{th} absorption line for oxygen / water vapor
F_i	Absorption line shape factor for oxygen / water vapor
γ	Specific gaseous attenuation (dB/km)
γ_o	Specific gaseous attenuation due to dry air (dB/km)
γ_w	Specific gaseous attenuation due to water vapor (dB/km)
P_T	Transmitter Power (W)
ϕ_{TM}	Phase of GMSK signal
ϕ_{RG}	Phase of PN Ranging signal

List of Abbreviations

C&DH	Command and Data Handling
TT&C	Telemetry Tracking and Command
COTS	Commercial off-the-shelf
IMU	Inertial Measurement Unit
Mbps	Megabits per second
MB	Megabytes
OS	Operating System
I/O	Input/output
CAN	Controller Area Network
RTOS	Real-Time Operating System
RF	Radio Frequency
BER	Bit Error Rate
SNR	Signal-to-Noise Ratio
SSD	Solid State Drive
GMSK	Gaussian Minimum Shift Keying
QAM	Quadrature Amplitude Modulation
FSK	Frequency Shift Keying
PSK	Phase Shift Keying
PSD	Power Spectral Density
PDF	Probability Density Function

1 Introduction

Command and Data Handling (C&DH) and Telemetry Tracking and Command (TT&C) subsystems serve as the central nervous system and communicative link, respectively, for a spacecraft mission. In essence, C&DH manages the collection, processing, and routing of data between onboard instruments and components, and executes control commands, whilst TT&C operates the transmission and reception of data between the spacecraft and Earth-based control stations.

Space HAVEN's primary objective is to enhance Technology Readiness Level (TRL) of HATHOR[2] via an Earth-demonstrator mission. The C&DH and TT&C subsystems play crucial roles in ensuring the success of the demonstrator mission, from the ejection from the launch vehicle at 100 km altitude to touchdown, as illustrated in the mission profile (Figure 1). Notably, they facilitate the deployment of the foldable pattern into a fully open configuration at apogee (around 320 km), the active attitude control via reaction wheels for appropriate reentry orientation (Phase A)[3], the operation of the Thermal Protection System (TPS)[4] and the guided navigation control using moving block mass actuation (Phase B)[5]. Additionally, they record valuable data during the tumbling or unstable motions in Phase C for future dynamic analysis [6] and finally trigger parachute deployment for a soft landing (Phase D)[7].

As shown in Figure 1, the mission requires C&DH and TT&C subsystems to function seamlessly and actively monitor the demonstrator across all mission segments. Consequently, these systems must adhere to a high TRL to guarantee mission success. Following discussions with project coordinators[8] and other subteams, the TRLs for the C&DH and TT&C subsystems were set at 7 and 5, respectively. This decision aimed at securing reliable onboard and ground communications through the extensive use of Commercial Off-The-Shelf (COTS) components, whilst also providing scalability for future Mars missions, thus achieving cost-effective mission expansions.

This report focuses on the design of the C&DH and TT&C subsystems. The C&DH section discusses data budget estimation, selection of an appropriate bus system, and integration with other demonstrator subsystems. The TT&C section delves into the choice of a suitable modulation method and a quantitative analysis of communication downlink to inform the design of a ground station.

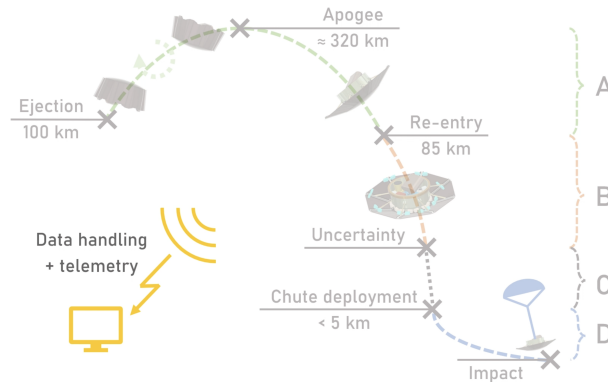


Figure 1: Demonstrator Mission Profile

2 Command & Data Handling (C&DH) Subsystem

2.1 Design Objectives and Requirements

The C&DH subsystem aims to establish robust, efficient communication among onboard avionics, encompassing data acquisition, actuator command executions, and mission-critical operations triggering of launcher ejection and parachute. Key objectives include data rate and size estimation, appropriate bus system selection, and efficient system architecture design with task distribution. Specific requirements are to store altitude-tagged telecommands for ejection, deployment, and active controllers in an autonomous process, append timestamps to locally acquired data for ordered timeseries, and utilise radiation-resistant Commercial Off-The-Shelf (COTS) products tested in previous missions, achieving a TRL of 7.

2.2 Data Budget Estimations

The design of a reliable and efficient system architecture requires a comprehensive data budget to manage the acquisition of data from onboard sensors and the execution of active control commands. These commands in-

clude the ejection signal, unfolding deployment trigger, reorientation attitude control, guided navigation descent, and the final parachute deployment. Note that the launch vehicle ejection, unfolding pattern deployment and parachute trigger commands are binary signals, so they do not factor into the data budget estimations. This budget only includes the raw data and their timestamps, but not communication overheads and error detection method information, such as a checksum, as these are bus-specific, which will be addressed in later sections.

The required data rate¹ of a sensor or for a active controller can be calculated as

$$\text{Data Rate (bit/sec)} = \text{Quantity} \times \text{Update Rate (Hz)} \times \text{Packet Size (bit)} \quad (1)$$

And the total data size can be calculated as

$$\text{Data Size (byte)} = \text{Quantity} \times \text{Update Rate (Hz)} \times \text{Packet Size (byte)} \times \text{Operating Time (s)} \quad (2)$$

Data budget summary tables for all components are shown in Table 1 and 2. For the sensors, the update rate can be found in their product datasheets [9][10], indicating the frequency at which refreshed new data are available, and the packet sizes were estimated based on the number of outputs each sensor generates. For instance, the star sensor has 4 values for quaternions and 3 values for angular rates. Each value is represented by an 8-byte double precision floating point number², and a timestamp of 4-byte unsigned integer is attached for each packet. Therefore, the star sensor outputs a data packet of 60 bytes.

Additionally, for the two active controllers the update rates were selected based on the frequency needed to update the control commands and state feedback, as per discussions with the Attitude and Navigation Control team members. In Navigation control, the data come from sending commands to 16 block actuators, while Attitude control involves sending commands to 4 reaction wheels. In each data packet, it includes a 2-byte unsigned integer for the command identifier, a 4-byte unsigned integer for the timestamp, and an 8-byte double-precision floating point number for desired control states, which added up to a packet size of 14 bytes.

Table 1: List of data considered in data budget estimations

Type	Item	Quantity	Update rate (Hz)	Packet size (bytes)	On time (s)
Sensors	IMU	3	800	52	3600
	GPS	3	400	36	3600
	Star Sensor	2	2	60	3600
	Heat sensor	16	5	12	3600
Commands	Navigation	16	100	12	50
	Attitude	4	100	12	360

¹Be sure to distinguish between Mb/s (a.k.a Mbps and Mbit/s) with MB/s (Megabytes/s). This mistake caused the painful complete redesign of C&DH from scratch, changing everything for the whole system!

²If single-precision were chosen, this leads to a data rate of 1.24 Mbps and a total data size of 556 MB. The Influence was rather tiny for a short mission like this. Hence, double-precision were chosen for better accuracy of results.

Table 2: Data rate and total data size estimations

Type	Item	Data Rate (Mbps)	Total Data Size (MB)
Sensors	IMU	0.9984	449.28
	GPS	0.3456	155.52
	Star Sensor	0.00192	0.864
Commands	Heat sensor	0.00768	3.456
	Navigation	0.1792	1.12
	Attitude	0.0448	2.016
	Total	1.5776	612.256

2.3 Bus, Operating System (OS), and Processors

Having estimated the required data rate and size, the next step is to choose a bus to link the onboard components. A bus serves as a communication system that transfers data between components. Within the context of computers, a bus defines the communication protocol, linking all components such as CPUs, memory modules, and I/O devices within a computer or between different computers. However, in a broader context within the C&DH subsystem, it facilitates communication and sets up the protocol between onboard processors, mass memory modules, and data acquisition from sensors. It also executes actuator commands and triggers deployment mechanisms based on sensor data, both in a hardware and software sense.

The choice of bus directly affects the design of architecture of C&DH subsystem itself and how it relates to the rest of demonstrator subsystems, including telemetry, navigation, attitude, and recovery systems.

6 different potential bus systems - SpaceWire, Gigabit Ethernet, Controller Area Network (CAN), MIL-STD-1553 - were studied compared. The detailed pros and cons of each bus system are summarised in table 3 in the Appendix. Finally, SpaceWire was chosen for its high data rate (2-200 Mbps for each link between the nodes e.g. sensors, processors, SSDs), low-power consumption, and its flexible architecture. Compared to CAN, for example, SpaceWire allows addition of further nodes or new subsystems without the need for significant reconfiguration of system architecture. Unlike Gigabit Ethernet, which requires significant overhead for packet routing and collision detection, SpaceWire's routing switches [11] provide direct point-to-point connections between the components. Furthermore, SpaceWire has a build-in error detection and recovery mechanism.

A real-time operating system (RTOS) is essential for Space Haven to ensure the timely execution of data collection tasks and control commands. RTEMS, an RTOS supported by SpaceWire [12], was therefore chosen.

Lastly, the choice of processor must also align with the chosen bus and OS. In this case, the LEON processor series, often used in space applications due to its fault-tolerance, radiation resistance and power efficiency, was chosen. LEON processors supports the SpaceWire protocol natively [13] and is compatible with RTEMS, making them well suited for system integrations later on.

2.4 System Integrations

Before discussing the overall C&DH system integration topology, it is pertinent to explain the general principles for designing SpaceWire-based communication systems. These guidelines are based on the user guide provided by Star-Dundee[14], a commercial provider of SpaceWire technology.

As shown in Figure 2, a SpaceWire data packet comprises a destination address, a cargo (which contains the raw data bytes and their respective timestamps as detailed in Tables 1), and an "End of Packet" marker.



Figure 2: SpaceWire Data Packet Format

A typical point-to-point link in SpaceWire, as illustrated in Figure 3, is full-duplex, bi-directional, and operates at a data rate of 2 - 200 Mbps, contingent on specific configurations. However, as the system complexity increases (see Figure 4), the architecture becomes convoluted, and the link bandwidth is not optimally utilised. Besides, this setup lacks redundancy.

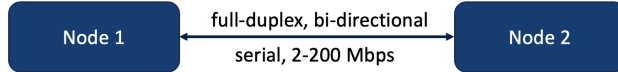


Figure 3: SpaceWire’s Point-to-point Link

To address these inefficiencies and enable effective communication among the components, a SpaceWire router (Figure 5) is introduced. The switch matrix inside the router can direct and guide packets arriving at one link interface to the other interconnected link interface. Consider the active attitude control subsystem that operates the reaction wheels, for instance. The GPS modules (Instrument 1) continuously collect altitude data at a frequency of 400 Hz and transmit this data to the SSD-based Mass Memory Module (MMM) via the SpaceWire router. Simultaneously, the onboard processor, also connected to the SpaceWire network, consistently monitors this altitude data through the flight software. Upon reaching a predefined altitude threshold, the processor dispenses control commands at a frequency of 100 Hz to the reaction wheels (Instrument 2) to make the necessary adjustments. These adjustments are made based on the attitude data collected from the sun and star sensors (Instrument 3). This operation repeats throughout the attitude control segment and is programmed to terminate automatically once the demonstrator reaches the desired attitude for reentry into the atmosphere. This desired state is verified when the processor reads the requisite attitude information from the SSD, supplied by the star and sun sensors.

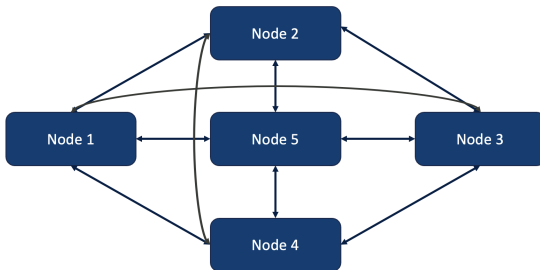


Figure 4: Purely Point-to-Point Link Connections Between Nodes

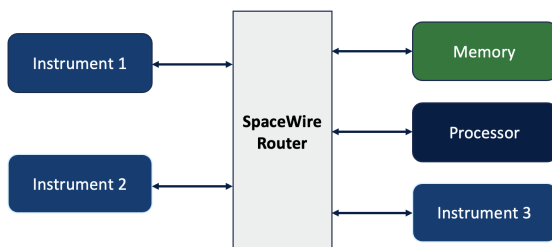


Figure 5: SpaceWire’s Router-Based Architecture

As the network structure for SpaceWire-based communications can be quite flexible, the design of C&DH system integrations can vary significantly, as demonstrated by different missions such as ESA’s ExoMars [15], NASA’s Lunar Reconnaissance Orbiter[16], and ESA and Japan Aerospace Exploration Agency’s BepiColombo Mercury Mission [17].

Figure 6 depicts the overall C&DH subsystem architecture. To distribute the workload, two LEON microprocessors were chosen to function concurrently for different tasks. Rather than designating a primary or redundant processor, a fault-tolerant network was established. If one processor encounters an error, the system can utilise the other processor to execute the corresponding commands since all nodes are interconnected.

For the thermal protection system (TPS) testing, as there is no active thermal control system in the demonstrator, heat sensor data are sent directly to the two mass memory modules. In addition, redundant IMU + GPS data are stored in these modules. Given SpaceWire’s point-to-point link, this data, which is not part of the active control mechanisms, can be streamed directly into the solid-state drive (SSD) mass memory modules as well.

Processor 1 primarily manages the deployment of unfolding panels and guided reentry navigation control. The execution of these commands requires direct information from the combined IMU+GPS sensor module, routed via SpaceWire Router 1. On the other hand, Processor 2 handles ejection from the launch vehicle, attitude control, and triggers the parachute mortar via SpaceWire Router 2. Due to the parachute mortar’s weight of 2.2 kg, only one unit was included. However, to maintain redundancy, two ignition leads are designed [7]. The redundant ignition lead is attached to SpaceWire Router 1.

To reduce network traffic, Processors 1 and 2 alternately handle control commands and telemetry transmission (To be discussed in the next section) or act as a redundancy backup. The real-time telemetry corresponds to the processor and router currently in charge of processing.

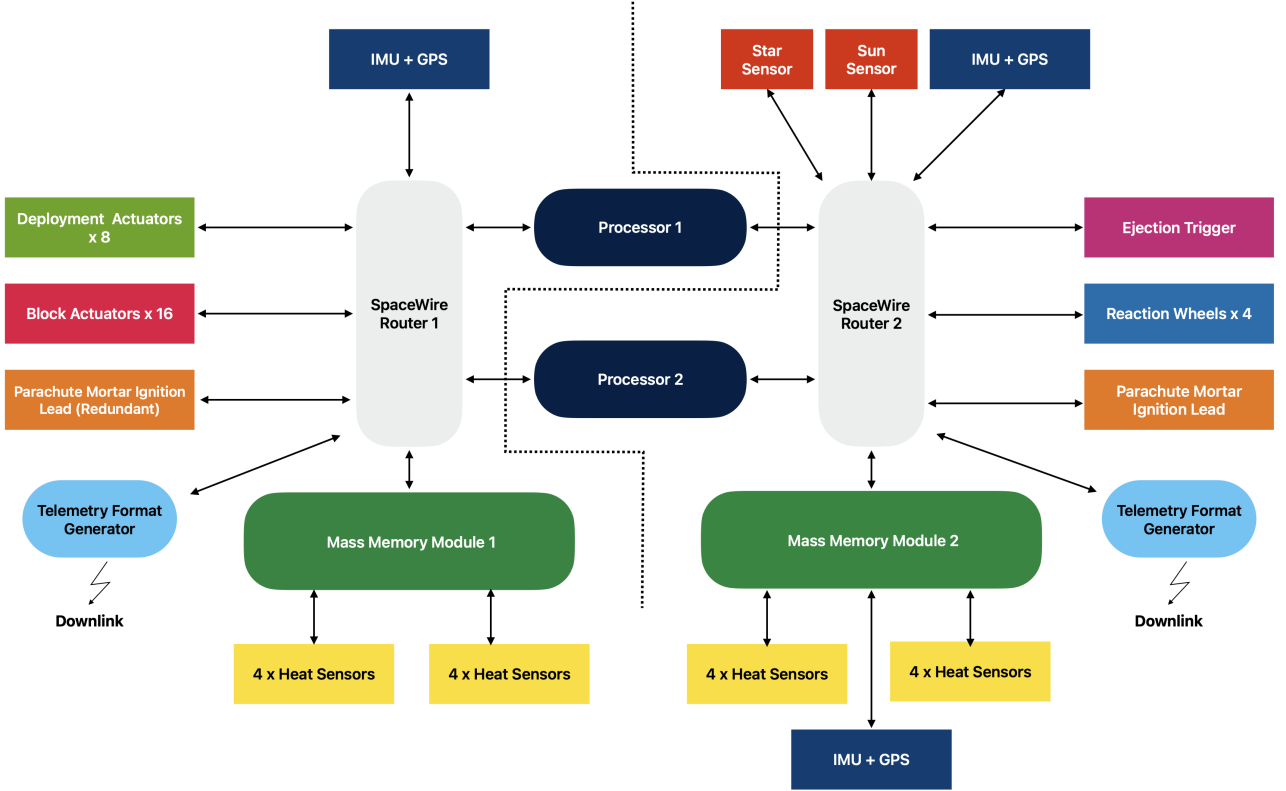


Figure 6: C&DH Subsystem Architecture

3 Telemetry Tracking & Command (TT&C) Subsystem

3.1 Design Objectives and Requirements

In the design of TT&C subsystem, the primary aim is to develop a robust communication link , aiming at a TRL of 5, compatible with standard recommended by Consultative Committee for Space Data Systems (CCSDS) to satisfy the regulations, that can maintain integrity under extreme re-entry conditions, transmitting crucial deployment status and real-time data read from the sensors, including IMU, GPS, star sensors, and contact heat sensors to the ground station using radio frequencies (RF). These data serve as an important role in providing insights into demonstrator performance. TT&C also acts as a redundancy module to onboard Solid-State Drive (SSD) data storage in crash analysis, as the data transmitted by telemetry can be recovered right before the instant of crash,in the order of milliseconds, depending on the data sampling rate of the specific sensors (Table 1).

A number of critical requirements were taken into account to ensure reliable and robust data transmission during the mission. The accuracy of the transmitted data received in the ground station is quantified by the probability of error in any one bit, i.e., *bit error rate* (BER). For typical transmission systems, a good BER is in the range of 10^{-9} to 10^{-3} [1]. Furthermore, noise voltage generated in the ground receiver, combining with the communication channel attenuation, can be large enough to cause the output to fall into the wrong side of digital bits of 0s and 1s, causing an error in retrieving the data. Therefore, a high *Signal-to-noise ratio* (SNR), calculated by the ratio of signal power to noise power, at least greater than 10 dB should also be considered to ensure a to ensure a high-performing tracking[18].

Simulink was utilised to simulate the communication link between the onboard transmitter to the ground receiver for the entire duration of mission to account for the conditions encountered in the downlink communication process, including the local environment conditions, loss and shift, noise in electronic components, while following the reentry trajectory. However, the uplink communication process was not included as a decision of the subgroup, as the navigation and attitude control systems and the parachute deployment was designed to be fully autonomous at desired altitude.

3.2 Reentry Environment and Atmospheric Conditions

Historically, blackouts had long roots of problems in radio communications for high-speed reentry vehicles. During hypersonic reentry, an ionised plasma layer is generated by the shock-heated air around the demonstrator. The plasma sheath acts as an insulator, trapping heat and raising the surface temperature of the demonstrator, potentially posing a potential challenge for the TPS design. Detailed analysis of this for Space HAVEN mission, including the heat fluxes and loads of Space HAVEN demonstrator compared to those of ADEPT [19] and MINI-IRENE [20], can be found in the Aerodynamics analysis [21] and TPS design [4]. In the context of radio communications, the radio signal generated by the onboard transmitter is either significantly attenuated or completely blocked as the plasma sheath can reflect, absorb, or scatter radio waves, interrupting the communication between the demonstrator and the ground station [22].

However, the period of blackout can be largely shortened by a proper choice of carrier frequency, or can be fully avoided by choosing an appropriate carrier frequency. Lower frequency waves (VHF, UHF bands) are affected more severely, which might lead to a complete blackout [23]. Higher frequency waves, such as those in the order of GHz, are less affected and can penetrate a certain depth of the plasma sheath, albeit with an attenuation in strength on the order of 10^1 to 10^2 dB, since their wavelengths are shorter than the Debye length of the plasma sheath[24]. The plasma frequency ω_p is calculated as

$$\omega_p = \sqrt{\frac{n_e e^2}{\epsilon_0 m_e}} \quad (3)$$

where n_e is the electron number density (x -axis in Figure 7), $e = 1.602 \times 10^9$ C is the elementary charge, m_e is the electron mass, and ϵ_0 is electric constant in free space (vacuum permittivity). And for the radiowave to penetrate, it is required that the carrier angular frequency $\omega > \omega_p$ or $f_c > \omega_p/2\pi$. Figure 7 shows the relationship between the carrier Radio Frequency (RF) it requires to penetrate the plasma sheath to avoid blackouts. However, equation 3 assumes the plasmas themselves are collisionless, hence giving an underestimate of the carrier frequency. Nonetheless, it approximately predicts the order of RF needed [24]. Note that n_e , chosen to vary between 10^9 to 10^{14} cm $^{-3}$, was based on empirical testings and empirical data obtained from NASA's Radio Attenuation Measurements (RAM) program[23]. The attenuation α through plasma sheath can be approximated using

$$\alpha = k_0 \left[-1 + \frac{\omega_p^2}{\omega^2 + \nu^2} + \sqrt{\left(1 - \frac{\omega_p}{\omega^2 + \nu^2}\right)^2 + \left(\frac{\nu}{\omega} \frac{\omega_p^2}{\omega^2 + \nu^2}\right)^{\frac{1}{2}}} \right]^{\frac{1}{2}} \quad (4)$$

where k_0 is the wave number in free space, $\nu = 3 \times 10^8 \frac{\rho}{\rho_0} T_p$ is plasma collision frequency. Results are shown in 8 assuming a plasma temperature of $T_p = 5000$ K as in RAM mission [25], as this information is unavailable for Space HAVEN. The plasma sheath depths, obtained from the Langmuir probe of RAM, were between 0 to 14 cm depending on altitudes and local electron number densities, indicating that maximum attenuations of 279 dB for C-band, 172 dB for S-band, and 30.6 dB are expected at 30.6 km (details shown in Appendix in Figure 19). Note that RAM was conducted at a reentry speed of 7620 m/s in the 1960s and 1970s (vs Space HAVEN: 2119 m/s). So Space HAVEN should expect lesser effect from plasma. The above attenuations are overestimations. Despite plasma attenuation, by making appropriate choices for transmitter and receiver gains, real-time telemetry for Space HAVEN can be achieved with minimal blackout influence.

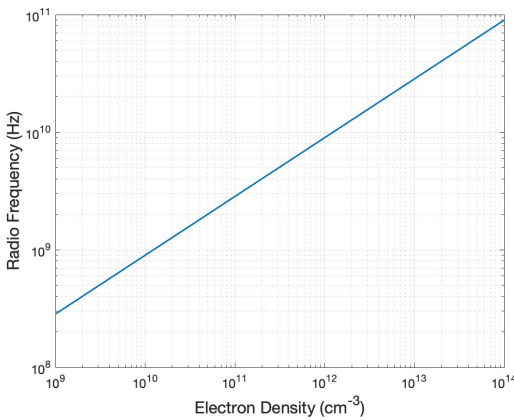


Figure 7: Required carrier frequency to penetrate the plasma sheath at a given Electron density

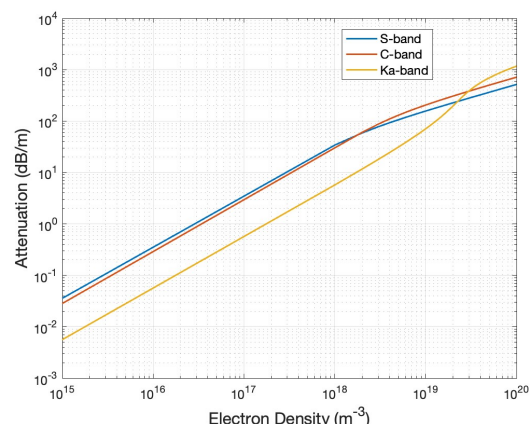


Figure 8: Radiowave Attenuation vs Electron Density

3.3 System Architecture



Figure 9: High-level TT&C System Architecture

The TT&C subsystem comprises three main sections: the onboard transmitter, the communication downlink channel, and the ground station receiver, as shown in Figure 9. As agreed upon by the team, there will be no uplink communication between the ground station receiver and the demonstrator during the mission since the controllers are designed to be fully autonomous. The following sections will first evaluate the losses and shifts occurring in the communication channel, then select a suitable data modulation method, and finally present the design logic of the ground station receiver. RF carrier frequency was decided to be S-band of 3GHz, in accordance with CCSDS's Category A vehicles [26].

3.4 Communication Channel

Free space loss L_s , often expressed as an attenuation in decibels, refers to the reduction in signal power density in an electromagnetic wave with a carrier frequency of f_s as it propagates through free space. This occurs as the wave spreads out from its source: the antenna of the transmitter aboard the demonstrator, to the receiving antenna located on the ground. The extent of this loss is dependent on the distance r between these antennas calculated using Haversine formula by the Mission Analysis Team [27], the carrier frequency f_s of the signal and the speed of light c , as shown in Equation 5.

For simplicity in the calculation, it was assumed that the antennas for both the onboard transmitter and ground receiver were isotropic. An isotropic antenna is a theoretical antenna which radiates and receives power uniformly in all directions. In real-world scenarios, antennas are directional, having higher gains in the main lobe direction and considerably lower gains in the side lobe direction. Regardless, Equation 5 properly estimates the order of magnitude of attenuation.

$$L_s = 20 \log_{10}\left(\frac{4\pi r}{c}\right) + 20 \log_{10} f_s \text{ (dB)} \quad (5)$$

The Doppler effect is particularly significant in a reentry context for the mission due to the high and rapidly changing relative velocities between the demonstrator v_s and the stationary ground station $v_o = 0$. As shown in Equation 6, the observer frequency f_o can be calculated and it is lower than the carrier frequency for the vehicle is moving towards the ground. The Doppler shift is the difference in frequencies between the ground receiver and the demonstrator, shown in equation 7. Figure 11 shows the varying shift in Hertz with respect to mission time. This necessitates frequency correction at the ground station for successful data recovery.

$$f_o = \frac{c + v_o}{c + v_s} f_s \quad (6)$$

$$f_d = f_o - f_s = -\frac{v_s}{c + v_s} f_s \quad (7)$$

Additionally, when RF propagates through the atmosphere, a small amount of attenuation can happen due to the absorption lines of atmospheric gases, primarily by dry air (mainly the large contribution of oxygen), as well as a small contribution of pressure-induced nitrogen attenuation, and water vapor. For carrier frequency less than 1000 GHz, the specific atmospheric attenuation can be accurately calculated by International Telecommunication Union's ITU-R P.676-12 Model [28], using Equations 8, 9, and 10.

$$\gamma = \gamma_o + \gamma_w = 0.1820 f (N''_{oxygen}(f) + N''_{water vapor}(f)) \text{ (dB/km)} \quad (8)$$

$$N''_{oxygen}(f) = \sum_{i(oxygen)} S_i F_i + N''_D(f) \quad (9)$$

$$N''_{water vapor}(f) = \sum_{i(water vapor)} S_i F_i \quad (10)$$

where N''_{oxygen} , $N''_{water vapor}$, and N''_D are the imaginary parts of the complex refractivities of oxygen, water vapor, and pressure-induced nitrogen, respectively. And S_i is the strength of the i^{th} absorption line for oxygen

or water vapor, while F_i is their corresponding absorption line shape factor. As the attenuation from Nitrogen molecules is small compared to that of oxygen, it is a convention to include it within the calculation as with oxygen. Values of these variables can be found in [28].

The effects of other factors, such as atmospheric refraction (which can cause slight shifts in the apparent elevation angle of the demonstrator) and polarisation, are minimal [29] and therefore were not considered in this report.

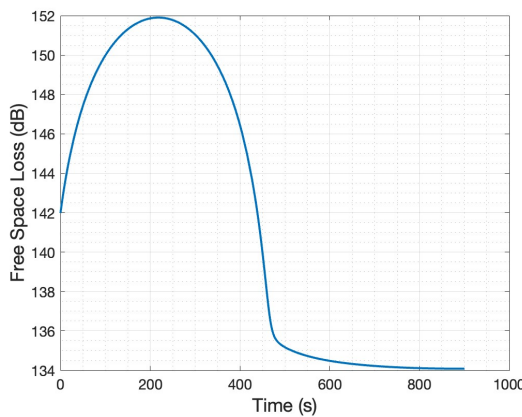


Figure 10: Free space loss vs Mission time

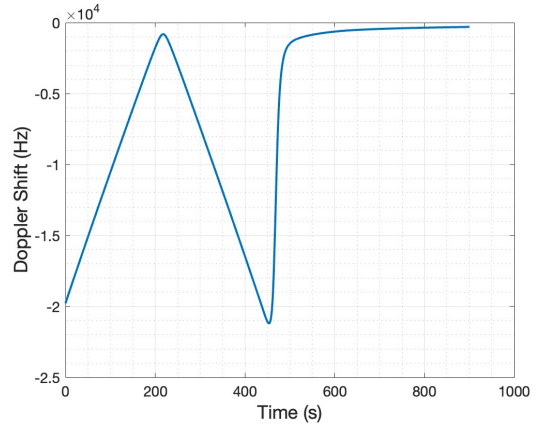


Figure 11: Doppler Shift vs Mission Time

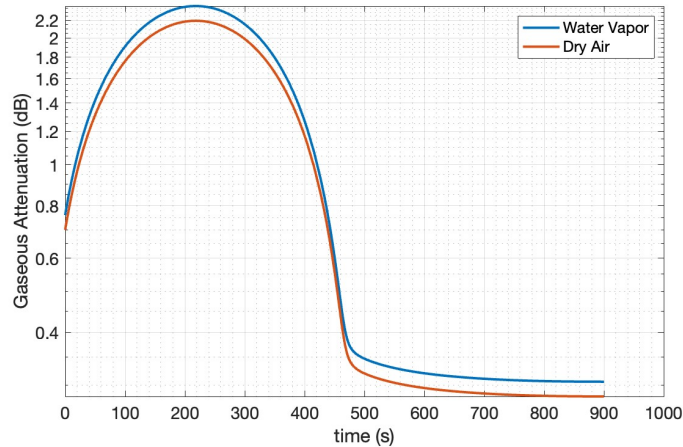


Figure 12: Atmospheric Attenuation vs Mission Time

As seen in Figures 10, 11, and 12, free space loss and Doppler shift significantly impact ground station design, with atmospheric attenuation has a lesser influence. Free space loss informs the data modulation method and gain requirements for onboard transmitters and ground station receivers. The Doppler effect presents challenges in correctly recovering encoded data signal at the ground station.

3.5 Data Modulation Method: GMSK

Data modulation is an essential process in data transmission using RF, which involves varying a carrier signal to create a waveform that can carry information, as the raw data in their original forms are not suitable for RF transmission due to their inherent low frequencies. For example, the signal of a television can be in order of a few tens of Hz to a few MHz, which are not transmittable themselves without a modulation to a higher carrier frequency.

In the context of the Space HAVEN's demonstrator mission, signal attenuation and distortion are significant challenges due to the operational environment in a reentry trajectory, with rapidly changing altitudes and velocities, in the mission duration of approximately 900 seconds in total. Noise and synchronisation issues between the on-board transmitter and ground station also need consideration. Several modulation methods compatible with CCSDS's standards, such as Phase Shift Keying (PSK) and Quadrature Amplitude Modulation (QAM) were considered as potential candidates [26][30], but Gaussian Minimum Shift Keying (GMSK) was chosen for this mission.

GMSK, a derivative of Frequency Shift Keying (FSK), incorporates a Gaussian filter, making it resistant to noise and signal distortion, less susceptible to signal attenuation, and suitable for bandwidth spectral efficiency and low power consumption, making it a more suitable method for this mission than other aforementioned candidates. Furthermore, Pseudo-Noise (PN) ranging was utilised to facilitate frame synchronisation and time recovery, a critical aspect in reliable communication [31]. PN ranging provides a unique token at the start of a data packet, ensuring synchronisation. This is achieved by using the same polynomial to generate a PN sequence for both modulation and demodulation processes. For this mission, a 64-bit PN sequence of $z^6 + z + 1$ was chosen for its superior noise and interference rejection capabilities.

Notably, the application of GMSK in space missions is a relatively new but growing trend, with potential for extending to Deep Space missions. This implies that the telemetry system designed here could be potentially upscaled for future missions to Mars [32], achieving a cost-effective mission expansion.

Mathematically, the modulated RF carrier signal ready to be sent via the downlink communication channel can be expressed as

$$x(t) = \sqrt{2P_T} \cos[2\pi f_c t + \phi_{TM}(t - \tau_{TM}) + \phi_{RG}(t - \tau_{RG})] \quad (11)$$

In this equation, $\phi_{TM}(t)$ and $\phi_{RG}(t)$ are the phases of the GMSK and PN ranging signals respectively, while τ_{TM} and τ_{RG} represent the asynchronous offsets between the telemetry and ranging signals, respectively. Here, f_c is the carrier frequency (selected to be in the 3GHz S-band), and P_T is the transmitter power.

Figure 13 demonstrates the implementation and recovery process of the modulation method described in Equation 11, using a Simulink model. The parameters in the model follow the CCSDS's standard as described in [33][26][30]. The transmitted signal was fully recovered in a test of 5000 bits, with a Bit Error Rate (BER) of 0 as expected - as there was no source of loss in between - and a transmission delay of 15 bits, as shown in Figure 14.

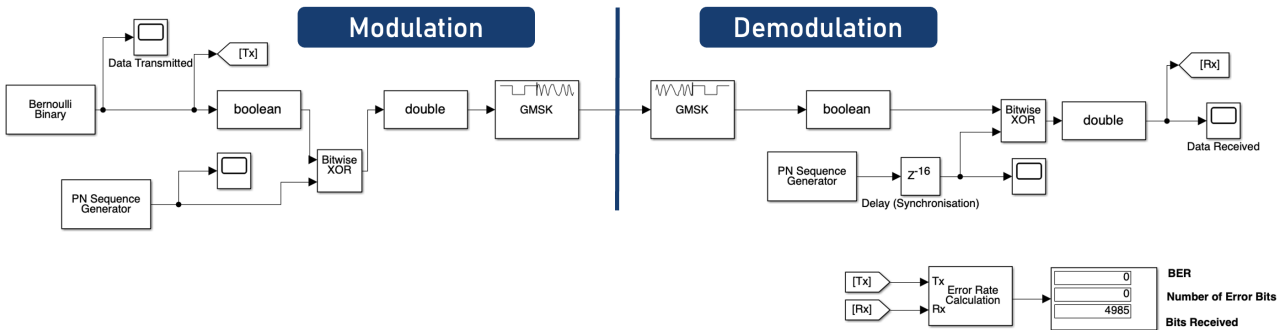


Figure 13: GMSK Data Modulation Method

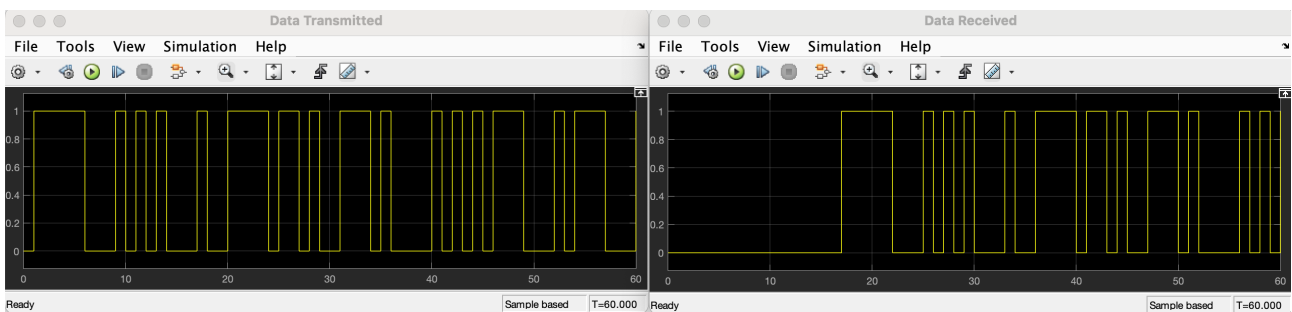


Figure 14: Encoded data signal transmitted and encoded signal data received at ground station with a delay

3.6 Ground Receiver Design

Figure 15 illustrates the power spectral density (PSD) of the modulated signal, before and after the downlink communication process over the mission. Essentially, the PSD provides a graphical representation of how the power of the signal is dispersed over varying frequencies offset from the carrier frequency. A peak at 0 kHz (Figure 18 might have a clear x-axis) is indicative of the majority of the signal power being concentrated at the

carrier frequency. This information becomes crucial when assessing the impact of losses and frequency shifts on the signal during downlink communication. Different frequencies may experience varying degrees of these effects, potentially causing uneven degradation of the signal quality.

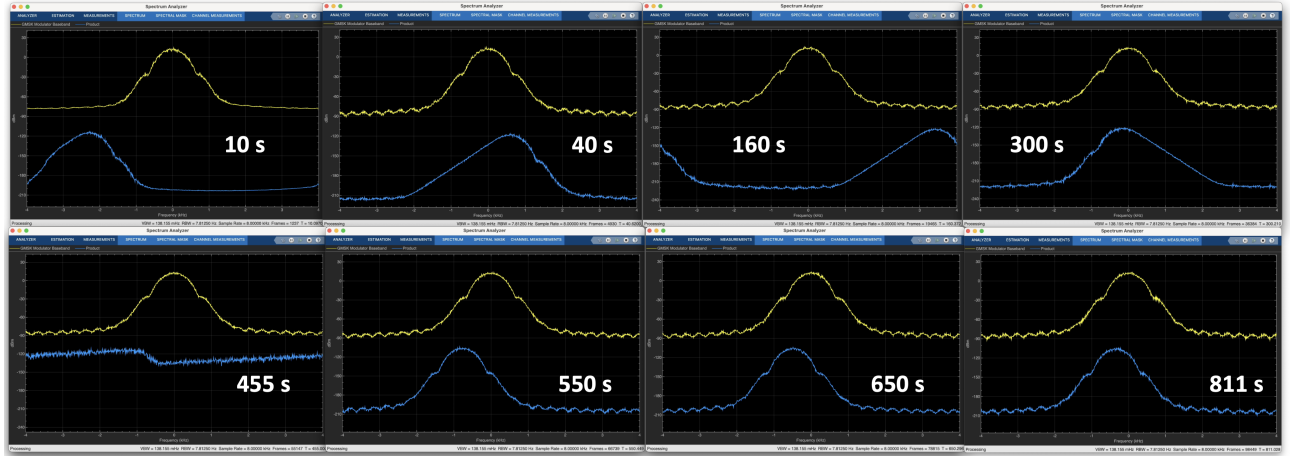


Figure 15: Power Spectral Density (dBm) Snippets of Before (yellow) and After the Downlink Process (blue)

In Figure 15, the yellow curve denotes the modulated signal output from the transmitter, whilst the blue curve represents the same signal after it has undergone the downlink process, but before the application of any gain amplifiers and phase corrections. It is clear that the downlink process incurs a reduction in the signal's PSD due to losses and shifts. Notably, between 300 to 500 seconds into the mission (as detailed in Figure 11 and 21), when the demonstrator achieves apogee and commences the reentry phase, the rapidly changing velocity imparts a particularly strong Doppler shift effect on the signal.

The major goal of the ground station receiver design is to mitigate the effects of signal degradation by amplifying the received signal and correcting any introduced frequency shifts and noise. Despite the inherent resistance to noise feature of GMSK + PN modulation, formulating a correction mechanism for the Doppler effect remains a significant task.

Two primary sources of noise were considered in this design: noise power generated within the receiver amplifier, and phase noise. The schematic mechanism for the former is depicted in Figure 16. Phase noise, on the other hand, originates from jitter (instabilities in the time domain), causing short-term and random fluctuations in the phase of the waveform. For practical purposes, the Probability Density Function (PDF) of noise can be approximated as a Gaussian distribution, described as:

$$P_n(x) = \frac{1}{\sigma_n \sqrt{2\pi}} \exp\left(\frac{-x^2}{2\sigma_n^2}\right) \quad (12)$$

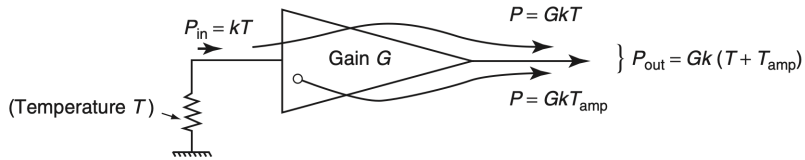


Figure 16: Definition of Noise Temperature [1]

Several strategies exist to tackle these issues, including predictive Doppler correction, which leverages known mission trajectory and velocity data, or the use of Software-Defined Radio (SDR). The latter can dynamically adjust the carrier frequency to accommodate the changing Doppler effect by tuning the local oscillator frequency in real-time [34]. Post-mission processing of the received data is another approach, though it does not provide real-time information and not suitable for Space HAVEN.

Without such corrective measures, the Bit Error Rate (BER) was found to increase to 0.59, which was ironically less reliable than random guessing of binary bits (0s and 1s). To rectify, a Proportional-Integral (PI) controller with $P = 29$ and $I = 5$ was designed and implemented at the ground station to provide controlled correction upon receipt of the transmitted data. The setup of this system is depicted in Figure 17. As shown in Figures 17 and 18, the signal was effectively recovered with a BER of 5.33×10^{-5} and a strong signal-to-noise ratio of 48.07

dB, with an onboard transmitting gain of 10 dB and ground receiving gain of 35 dB indicating of a satisfactory design.

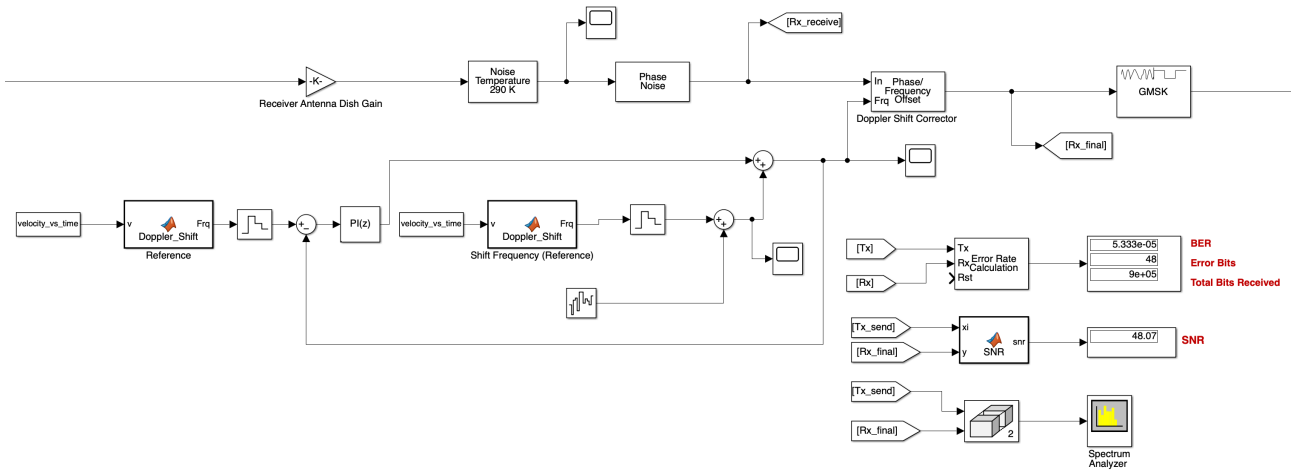


Figure 17: Ground Station Design in Simulink

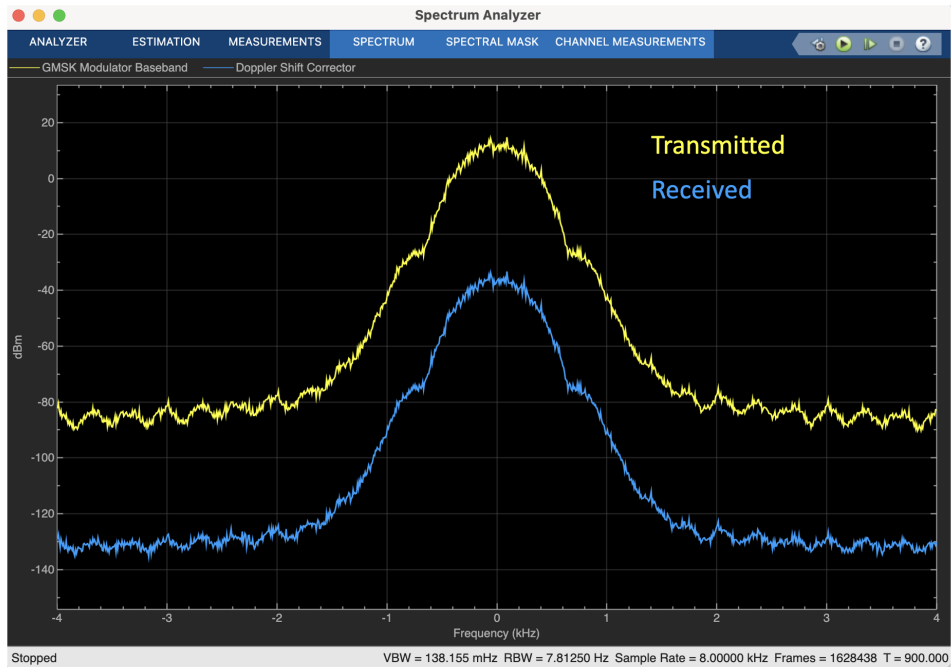


Figure 18: Power Spectral Density (dBm) after Doppler Corrections

4 Discussions and Future Works

4.1 C&DH Subsystem

C&DH subsystem as presented in this report represents a high-level design, primarily focusing on the architectural arrangement and integration of various demonstrator subsystem components. However, more in-depth work is essential for future endeavors. One such key area of focus would be the development of software functionalities for task scheduling, which is crucial to manage onboard activities and for ensuring efficient traffic handling in the SpaceWire network, to avoid data collisions and maintain seamless communication.

Real-life reentry missions, like the European Space Agency's Atmospheric Reentry Demonstrator, involve a substantially higher number of sensors and equipment, with more than 200 different parameters, including

121 temperature channels, 38 pressure channels, 14 accelerometers, 8 reflectometers, 5 force measurement channels, and an acoustic channel [35]. Besides, these missions also integrate various functional parameters such as mission sequences for better health monitoring and control. Future work should thus aim to incorporate and manage this complex mesh of data sources effectively within the C&DH subsystem.

Moreover, it is critical to give due importance to the protection of onboard avionics, as they remain essential to maintain the operations and stability of the vehicle. This could include advanced monitoring systems to detect and mitigate potential anomalies, protective coatings or casings, and the use of fault-tolerant designs to enhance the robustness of the overall system.

4.2 TT&C Subsystem

In this report, the antennas were modelled as isotropic radiators for the sake of simplification. Future work should focus on designing the antenna's actual beam shape and direction, which plays a significant role in determining signal coverage and strength. More detailed studies could be conducted in the selection of onboard transmitters and receivers, possibly using tools like MATLAB's RF Link Budget Analyzer app, which can provide a more comprehensive understanding of the overall system performance.

Hardware selection will also play a critical role in the system performance. Local components should be carefully selected and designed to accommodate for potential issues such as I/Q imbalance, DC offsets, and other non-idealities that might not have been fully captured in the Simulink model. Currently, the setup in Simulink is overly ideal with deliberately introduced randomness.

Finally, the TT&C subsystem should also consider the conditions prior to the actual demonstrator mission when it is still onboard the launcher. This involves different operational and environmental factors that may impact the system's performance, requiring additional layers of resilience and robustness in the design.

5 Conclusion

This report presents a comprehensive design for the Space HAVEN demonstrator's Command and Data Handling (C&DH) and Telemetry Tracking and Command (TT&C) subsystems.

The C&DH design was initiated with a meticulous data budget analysis that accounted for all components across various demonstrator subsystems. These included unfolding pattern deployment, attitude control, guided navigation reentry control, recovery system, and telemetry system. The analysis projected a data rate of 1.578 Mbps and a total size of 612.256 MB for the entire mission. The SpaceWire bus was selected for its high data rate, flexible network structure, and low power consumption. This decision was accompanied by the selection of the Real-time Operating System (RTOS) platform RTEMS and the LEON processor series, which supports RTOS. This combination of commercial off-the-shelf (COTS) components ensures the robust performance of the onboard system under the harsh conditions of space and reentry, and the reliable execution of mission tasks. It also attains a high Technology Readiness Level (TRL) of 7, ensuring successful mission testing and smooth autonomous control throughout. Detailed designs of communication and collaboration among processors, mass memory modules, sensors, and actuators were also covered in this report.

For the TT&C design, free-space and atmospheric losses, as well as Doppler shifts, were quantitatively evaluated for the communication link channel between the onboard transmitter and the ground station receiver, based on the mission profile provided by the mission analysis team. The Gaussian Minimum Shift Keying (GMSK) and Pseudo-Noise (PN) Ranging modulation method was selected for its noise and signal distortion resistance, as well as its bandwidth efficiency. An efficient ground station was designed to ensure reliable communication down-link. Various noise sources were considered and simulated in the model, with a PI controller designed to correct frequency distortion due to the Doppler effect. Ultimately, the receiver achieved a bit error rate (BER) of 5.33e-5 and a signal-to-noise (SNR) ratio of 48.07 dB, indicating a satisfactory design with a TRL of 5.

Acknowledgements

I would like to thank everyone in FAD group, with a special mention to Sevan, Cristian, Paula, and Shapol, with whom I have closely worked with for this project for the collaborative teamwork. I am grateful for our weekly meetings with our subteam supervisor Dr Bruce, whose feedback were constructive to guide C&DH and TT&C's designs tailored to be more specific to this mission rather than as a general design. Additionally, I want to thank the supervisors, Drs Cantwell, Santer, Lee, Steiros, and Profs Laizet and Aliabadi, for their helpful feedback and suggestions on aspects of the work that I had overlooked in the presentations.

References

- [1] P. Fortescue, G. Swinerd, and J. Stark, *Spacecraft Systems Engineering*. John Wiley & Sons, 2011.
- [2] D. O'Driscoll, M. Gramola, T. Wang, P. J. Bruce, and M. J. Santer, "Design, construction, and mechanical testing of a rigid-deployable aeroshell for atmospheric entry," in *AIAA SCITECH 2022 Forum*, 2022, p. 1621.
- [3] C. Vegas Medina, "Space HAVEN: Design of the Demonstrator Attitude Determination and Control System," Department of Aeronautics, Imperial College London, Tech. Rep., 2023.
- [4] T. Uyumaz, "Space HAVEN: Structural Thermal Analysis of a Deployable Aeroshell Demonstrator," Department of Aeronautics, Imperial College London, Tech. Rep., 2023.
- [5] P. Gutierrez, "Space HAVEN: Innovative control and navigation system using block mass movement for a foldable deployable aeroshell," Department of Aeronautics, Imperial College London, Tech. Rep., 2023.
- [6] Y. Dun, "Space HAVEN: Hypersonic and Supersonic Analysis of a Foldable Aeroshell Demonstrator," Department of Aeronautics, Imperial College London, Tech. Rep., 2023.
- [7] S. Vlieghe, "Space HAVEN: Design and Dynamic Modelling of a Parachute Recovery System," Department of Aeronautics, Imperial College London, Tech. Rep., 2023.
- [8] E. Lam, "Space HAVEN: Project Co-ordination, Market Analysis, Schedule Slippage Risks and Business Planning," Department of Aeronautics, Imperial College London, Tech. Rep., 2023.
- [9] VECTORNAV, "VN-200 GNSS/INS Datasheet," <https://www.vectornav.com/docs/default-source/datasheets/vn-200-datasheet-rev2.pdf>, accessed on June 15, 2023.
- [10] Rocket Lab, "Star Tracker ST-16RT2 Datasheet," <https://www.rocketlabusa.com/assets/Uploads/RL-ST16RT2-Data-Sheet.pdf>, 2021.
- [11] S. Parkes, C. McClements, G. Kempf, S. Fischer, and A. Leon, "Spacewire router," in *ISWS International SpaceWire Seminar 2003*, Noordwijk, The Netherlands, November 2003, pp. 180–187, accessed on June 9, 2023. [Online]. Available: <http://spacewire.esa.int/WG/SpaceWire/ISWS-proceedings/CD%20ISWS%202003/Presentations/7%20-%20SpaceWire%20Router.pdf>
- [12] Star Dundee, "Starwire bus and rtems system," https://www.star-dundee.com/products/star-system-for-rtems/#product_features, 2023, accessed on June 15, 2023. [Online]. Available: https://www.star-dundee.com/products/star-system-for-rtems/#product_features
- [13] STAR-Dundee, "High reliability network and data-handling technology for demanding applications," https://www.star-dundee.com/wp-content/star_uploads/product_resources/STAR-Dundee-Brochure.pdf, accessed on June 15, 2023.
- [14] S. Parkes, "Spacewire user's guide," https://www.star-dundee.com/wp-content/star_uploads/general/SpaceWire-Users-Guide.pdf, 2012, accessed on June 12, 2023.
- [15] B. Dean, R. Warren, and B. Boyes, "Rmap over spacewire on the exomars rover for direct memory access by instruments to mass memory," in *2nd International SpaceWire Conference*, Nara, Japan, November 2008, accessed on June 15, 2023. [Online]. Available: <http://2008.spacewire-conference.org/downloads/Papers/Missions%20&%20Applications%202/Dean.pdf>
- [16] J. Marshall, "Evolution and applications of system on a chip spacewire components for spaceborne missions," in *2nd International SpaceWire Conference*, Nara, Japan, November 2008. [Online]. Available: <http://2008.spacewire-conference.org/downloads/Papers/Components%202/Marshall.pdf>
- [17] S. Davy, C. McClements, S. Parkes, and T. Takashima, "Bepi colombo mmo data handling system spacewire-rmap interface," SpaceWire Working Group Meeting #11 June 10/11, 2008 – ESA/ESTEC, Space Systems Research Group, School of Computing, UoD, UK; LESIA, Observatoire de Paris, France; Department of Space Plasma Physics, ISAS/JAXA, Noordwijk, The Netherlands, June 2008, accessed on June 15, 2023. [Online]. Available: <http://spacewire.esa.int/WG/SpaceWire/SpW-SnP-WG-Mtg11-Proceedings/Presentations%20PDF/OoP-MMO-RMAPSpW-LESIA.pdf>

- [18] J. H. Yuen, *Deep Space Communications: An Introduction*. Jet Propulsion Laboratory, California Institute of Technology, 2014, ch. 1. [Online]. Available: https://descanso.jpl.nasa.gov/monograph/series13/DeepCommo_Chapter1--141029.pdf
- [19] A. Cassell, P. Wercinski, B. Smith, B. Yount, O. Nishioka, and C. Kruger, “Adept sounding rocket one flight test overview,” in *AIAA Aviation 2019 Forum*, 2019, p. 2896.
- [20] A. Fedele and S. Munguerra, “Aerodynamics and flight mechanics activities for a suborbital flight test of a deployable heat shield capsule,” *Acta Astronautica*, vol. 151, pp. 324–333, 2018. [Online]. Available: <https://doi.org/10.1016/j.actaastro.2018.05.044>
- [21] J. Tomas Pimentel, “Space HAVEN: Aerothermal heating analysis of a Foldable Aeroshell Demonstrator using analytical and Reduced Order Models,” Department of Aeronautics, Imperial College London, Tech. Rep., 2023.
- [22] R. Hartunian, G. Stewart, S. Fergason, T. Curtiss, R. Seibold *et al.*, “Causes and mitigation of radio frequency (RF) blackout during reentry of reusable launch vehicles,” Aerospace corporation, Tech. Rep., 2007. [Online]. Available: https://rosap.ntl.bts.gov/view/dot/12493/dot_12493_DS1.pdf
- [23] N. D. Akey and A. E. Cross, *Radio blackout alleviation and plasma diagnostic results from a 25,000 foot per second blunt-body reentry*. National Aeronautics and Space Administration, 1970.
- [24] M. Bachynski, “Electromagnetic wave penetration of reentry plasma sheaths,” *RADIO SCIENCE Journal of Research NBS/USNC-USRI*, vol. 69, no. 2, 1965.
- [25] R. P. Starkey, W. Santos, D. Hoult, and M. J. Lewis, “Plasma field telemetry for hypersonic flight,” MARYLAND UNIV COLLEGE PARK DEPT OF AEROSPACE ENGINEERING, Tech. Rep., 2003. [Online]. Available: <https://apps.dtic.mil/sti/pdfs/ADA430330.pdf>
- [26] Consultative Committee for Space Data Systems (CCSDS), “Radio frequency and modulation systems-part 1 earth stations and spacecraft,” 2016, accessed on June 12, 2023. [Online]. Available: <https://public.ccsds.org/Pubs/401x0b27s.pdf>
- [27] U. Yaqoob, “Space HAVEN: Foldable Aeroshell Re-entry Trajectory Planning and Optimisation,” Department of Aeronautics, Imperial College London, Tech. Rep., 2023.
- [28] International Telecommunication Union, “Attenuation by atmospheric gases and related effects,” *Recommendation ITU-R*, 2019. [Online]. Available: https://www.itu.int/dms_pubrec/itu-r/rec/p/R-REC-P.676-13-202208-I!!PDF-E.pdf
- [29] J. R. Wertz, D. F. Everett, and J. J. Puschell, *Space Mission Engineering: The New SMAD*. Space Technology Library, 2011. [Online]. Available: <http://www.sme-smad.com>
- [30] CCSDS, “Bandwidth-efficient modulations - summary of definition, implementation, and performance,” 2018, accessed on June 10, 2023. [Online]. Available: <https://public.ccsds.org/Pubs/413x0g3e1.pdf>
- [31] G. P. Calzolari, E. Vassallo, G. Sessler, and M. Visintin, “GMSK/PN for high rate telemetry and high accuracy ranging of Lagrange and Mars missions,” in *SpaceOps 2014 Conference*, 2014, p. 1851, accessed on June 9, 2023. [Online]. Available: <https://arc.aiaa.org/doi/pdf/10.2514/6.2014-1851>
- [32] S. Shambayati and D. K. Lee, “GMSK modulation for deep space applications,” in *2012 IEEE Aerospace Conference*, 2012, pp. 1–13.
- [33] CCSDS, “SIMULTANEOUS TRANSMISSION OF GMSK TELEMETRY AND PN RANGING,” 2021, accessed on June 11, 2023. [Online]. Available: <https://public.ccsds.org/Pubs/413x1g2.pdf>
- [34] K. Fisher, C. Jih, M. S. Moore, J. C. Price, B. A. Abbott, and J. A. Fritz, “Software-defined radio for space-to-space communications,” Tech. Rep., 2011.
- [35] D. Isakeit, A. Wilson, P. Watillon, T. Leveugle, C. Cazaux, and G. Bréard, “The atmospheric reentry demonstrator,” Tech. Rep., 1998. [Online]. Available: <https://www.esa.int/esapub/br/br138/br138.pdf>
- [36] D. Gwaltney and J. Briscoe, “Comparison of communication architectures for spacecraft modular avionics systems,” Tech. Rep., 2006.

- [37] Star-Dundee, “Missions Using Space Wire,” <https://www.star-dundee.com/spacewire/spacewire-users-guide/the-spacewire-data-handling-network/example-spacewire-mission-architectures/missions-using-spacewire/>, accessed on June 12, 2023.
- [38] NASA, “Orion reference guide,” https://www.nasa.gov/sites/default/files/atoms/files/orion_reference_guide_090622.pdf, 2022, accessed on June 12, 2023.
- [39] RENESAS, “Using can bus serial communications in space flight applications,” <https://www.renesas.com/us/en/document/whp/using-can-bus-serial-communications-space-flight-applications>.
- [40] C. Plummer, P. Roos, and L. Stagnaro, “CAN bus as a spacecraft onboard bus,” in *DASIA 2003-Data Systems In Aerospace*, vol. 532, 2003.

Appendix

Table 3: Comparison of Different Bus Systems

Bus System	Pros	Cons	Past Missions
SpaceWire[36][14] [37]	<ul style="list-style-type: none"> High data rate: 2 - 200 Mbps Flexible architecture to fit the mission requirements, instead of designing mission to fit architectural topology requirements Low-power consumption 	<ul style="list-style-type: none"> Limited availability of off-the-shelf components (Only from several companies, costs might be high) Limited Ground Support Equipment (GSE) for the time being 	Mars Reconnaissance Orbiter (2005), ExoMars(2016), James Webb Space Telescope(2021)
Gigabit Ethernet [36][38]	<ul style="list-style-type: none"> Extremely high data rate: 1000 Mbps Common standard 	<ul style="list-style-type: none"> Not many past missions High power consumption Heavy cables Susceptible to EM wave interference 	Orion Space-craft(2022)
CAN [39][40]	<ul style="list-style-type: none"> Well-established standard Message prioritisations Opensource platform for prototyping 	<ul style="list-style-type: none"> 1 Mbps Limited length, each data packet can only be a length of 8 bytes 	Mars Rover Curiosity (2011)
MIL-STD-1553[36]	<ul style="list-style-type: none"> Built-in error detection and correction Military Standard, proven in space Well-defined interface to handle command, status, and payload data 	<ul style="list-style-type: none"> Low data rate: 1 Mbps Legacy equipment Heavy due to dual-redundancy bus structures 	International Space Station (1998), Space shuttle Orbiter (1981-2011)

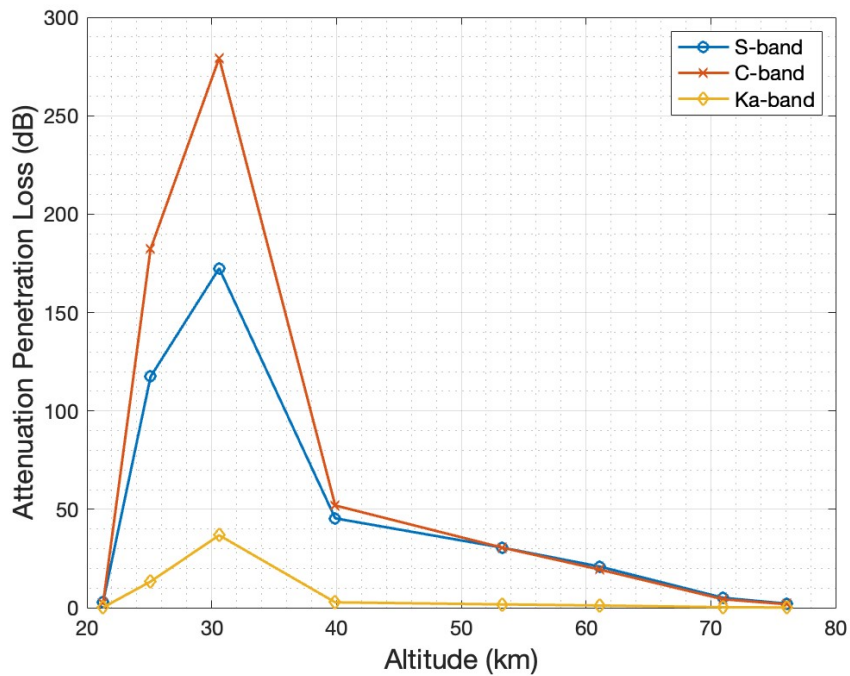


Figure 19: Attenuation due to Plasma Penetration vs Altitude for NASA's RAM mission

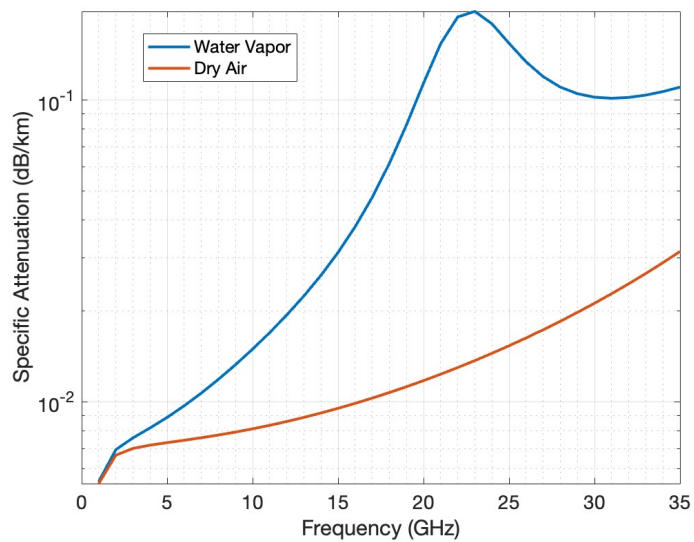


Figure 20: Specific Attenuation vs Carrier Frequency

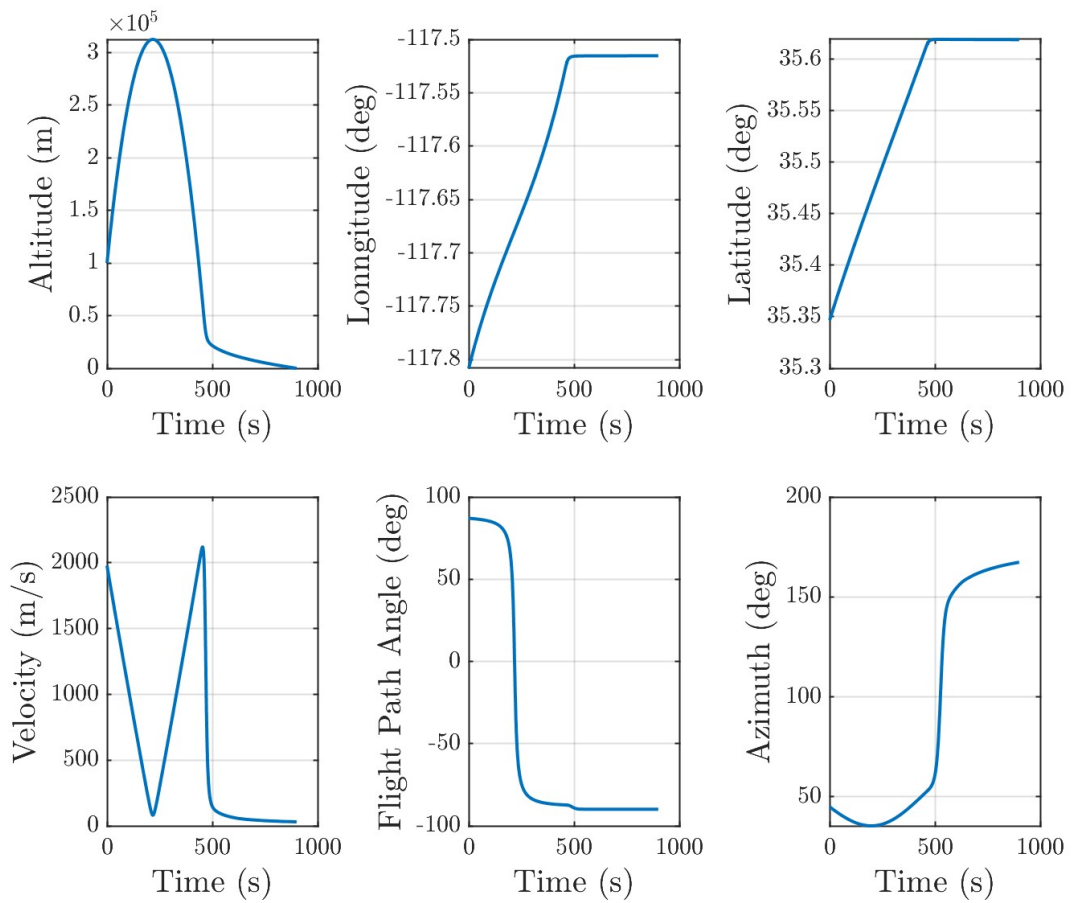


Figure 21: Demonstrator Reentry Trajectory from Mission Analysis Team